

Article

# Integrated the Artificial Potential Field with the Leader–Follower Approach for Unmanned Aerial Vehicles Cooperative Obstacle Avoidance

Yingxue Zhang <sup>1</sup>, Jinbao Chen <sup>1</sup>, Meng Chen <sup>1,2</sup>, Chuanzhi Chen <sup>1,\*</sup>, Zeyu Zhang <sup>1</sup> and Xiaokang Deng <sup>1</sup>

<sup>1</sup> College of Astronautics, Nanjing University of Aeronautics and Astronautics, Nanjing 211106, China; cherzhang0220@nuaa.edu.cn (Y.Z.); chenjbao@nuaa.edu.cn (J.C.); workmailcm@nuaa.edu.cn (M.C.); zhangzeyu@nuaa.edu.cn (Z.Z.); dengxk@nuaa.edu.cn (X.D.)

<sup>2</sup> Shanghai Key Laboratory of Spacecraft Mechanism, Shanghai 201109, China

\* Correspondence: czchen@nuaa.edu.cn

**Abstract:** For the formation and obstacle avoidance challenges of UAVs (unmanned aerial vehicles) in complex scenarios, this paper proposes an improved collaborative strategy based on APF (artificial potential field). This strategy combines graph theory, the Leader–Follower method, and APF. Firstly, we used graph theory to design formation topology and dynamically adjust the distances between UAVs in real time. Secondly, we introduced APF to avoid obstacles in complicated environments. This algorithm innovatively integrates the Leader–Follower formation method. The design of this attractive field is replaced by the leader’s attraction to the followers, overcoming the problem of unreachable targets in APF. Meanwhile, the introduced Leader–Follower mode reduces information exchange within the swarm, realizing a more efficient “few controlling many” paradigm. Afterwards, we incorporated rotational force to assist the swarm in breaking free from local minima. Ultimately, the stability of the integrated formation strategy was demonstrated using Lyapunov functions. The feasibility and effectiveness of the proposed strategy were validated across multiple platforms.

**Keywords:** UAV swarm; graph theory; APF; Leader–Follower method; rotational force; affine formation; reconfiguration

**MSC:** 5408; 9310



**Citation:** Zhang, Y.; Chen, J.; Chen, M.; Chen, C.; Zhang, Z.; Deng, X. Integrated the Artificial Potential Field with the Leader–Follower Approach for Unmanned Aerial Vehicles Cooperative Obstacle Avoidance. *Mathematics* **2024**, *12*, 954. <https://doi.org/10.3390/math12070954>

Academic Editor: Davide Valenti

Received: 8 February 2024

Revised: 8 March 2024

Accepted: 12 March 2024

Published: 23 March 2024



**Copyright:** © 2024 by the authors. Licensee MDPI, Basel, Switzerland. This article is an open access article distributed under the terms and conditions of the Creative Commons Attribution (CC BY) license (<https://creativecommons.org/licenses/by/4.0/>).

## 1. Introduction

As the task environment becomes increasingly complex, there is a growing demand for enhanced cluster control [1]. The control objectives now extend beyond the mere maintenance of formation stability and facilitation of effective formation changes. They now encompass the prevention of inter-agent collisions, secure navigation around obstacles, and other safety considerations. Presently, collaborative control of clusters has emerged as a central focus in current research. The utilization of multi-agent collaborative consensus theory [2] to investigate formation reconstruction, path planning [3], and obstacle avoidance within collaborative control has become a burgeoning area of study.

Common formation control methods encompass Leader–Follower approaches [4], behavior-based methods [5], APF approaches [6], virtual structure methods [7], and graph theory [8]. Graph theory methods have emerged as a novel approach in recent years for formation control. Leveraging graphs to depict topological relationships, this methodology transforms challenging problems within formations into a graphical representation. Consequently, this paper adopts a graph theory approach to fulfill fundamental formation tasks within swarms, utilizing its relevant knowledge [9] for the design of formation patterns and concurrently implementing affine transformations. In the face of increasingly complex task scenarios, there are obstacles everywhere. Therefore, how to avoid obstacles and reach the target point while coordinating the formation is a challenge in formation control strategy.

Scholars worldwide have conducted extensive research on the challenge of obstacle avoidance in multi-agent systems. Commonly employed obstacle avoidance algorithms encompass neural network approaches [10], ant colony algorithms [11], swarm intelligence algorithms, and APF methods [12]. Zhan et al. [13] employed a biased consistency neural network for distributed solving to obtain the shortest trajectory route. This method enables a highly parallel system with self-learning capabilities. Xia et al. [14] integrated the ant colony algorithm for global path planning with local obstacle avoidance rules, creating shorter and collision-free composite paths. Wang et al. [15] improved the foraging and elimination mechanisms in the bee colony algorithm, ensuring the simultaneous achievement of multi-objective optimization. A common issue among the aforementioned methods is a notable dependence on environmental information, leading to significant computational time. This dependency becomes particularly complicated when dealing with swarm formation. The APF method [16] presents an effective approach to mitigating collision issues within swarms. This method is characterized by its simplicity in design, low computational overhead, and high real-time performance. However, the challenges become evident when solely relying on the APF method [17]. First, it does not consider the collaborative relationships between UAVs. The second issue lies in the shortcomings of the method, such as local extrema and unreachable points [18].

In addressing the limitation of achieving collective collaboration under the influence of a single APF, this paper proposes a control strategy that integrates graph theory with APF. During the initial stages of formation, graph theory is employed to design corresponding topological configurations. The invariance of the topology is maintained based on the magnitude of the stress matrix, ensuring the safety distance between UAVs [19]. Based on the positive or negative values of the stress matrix, UAVs are either attracted to or repelled from each other, effectively preventing self-collisions among UAVs and ensuring that individual UAVs stay within the formation. When encountering obstacles, the APF method serves as the central approach for UAV collision avoidance, achieving spatial obstacle avoidance within the swarm. Building upon the proposed method in this paper, a swarm of UAVs can concurrently achieve formation control, inter-agent collision avoidance, and obstacle avoidance [20].

Addressing the inherent limitations in the APF method [21], the approach in [22] added virtual target points to modify the force equilibrium at those specific locations. Reference [23] introduced random disturbance components into the attractive potential field. Ref. [24] incorporated the path planned by the APF method as inspiration for the ant colony algorithm to conduct path searching. In [25], the Rapidly Exploring Random Tree (RRT) algorithm was introduced into the APF, treating nodes along the path as additional attraction sources while reducing the influence of the target point. However, the integration of the aforementioned methods tends to make the algorithm more complex, resulting in a higher computational load. Considering the computational and power constraints, this paper introduces rotational force into the foundation of the APF. This addition aims to overcome the challenges posed by local minima. In comparison to other algorithms, this method offers a smaller computational load, increased operability, and higher real-time performance.

The contributions of this paper are outlined as follows:

- (1) The combination of graph theory and APF methods demonstrates robust adaptability to environmental challenges.

Graph theory is an ingenious formation control method. However, its limitations make it challenging to handle scenarios with obstacles. To enhance the capabilities of cluster path planning and obstacle avoidance, this paper integrates the effective obstacle avoidance technique of the APF method into the formation control. Unlike other studies, the fusion control law designed in this paper is not limited to the control of a single variable; it takes into account the consistency of multiple variables within the swarm. This design results in stronger formation and coordination effects. After navigating through obstacles, the tracking error of the desired positions is minimized, leading to a more stable

formation configuration. In contrast to traditional APF, this paper considers inter-vehicle collaboration, resulting in enhanced adaptability to the environment.

- (2) Innovatively applying the Leader–Follower method overcomes the limitation of unreachable targets in the APF.

Typically, in APF methods, both an attractive field and a repulsive field are concurrently designed. However, when obstacles are present near the target point, the issue of unreachable targets may arise. This paper proposes integrating the Leader–Follower method into the APF, thereby eliminating the influence of the target point's attraction on the UAVs. In turn, the attraction force on the followers is replaced with the leader UAV. While following the leader, the follower simultaneously moves in the direction of the target point. It avoids the problem of unreachable locations in a different way.

- (3) By employing rotational force, the issue of APFs easily falling into local minima is addressed.

Although the APF method exhibits good obstacle avoidance capabilities, its drawbacks are quite apparent. One significant limitation is its susceptibility to becoming trapped in local minima points, causing the UAV to remain stationary due to force equilibrium. To address the issue of local minima encountered by APFs, a rotational force is introduced perpendicular to the force between the UAV and obstacles. The magnitude of this force is proportional to the repulsive force generated by the obstacles. Its direction remains parallel to the obstacles, allowing for smoother navigation around them. This additional force is applied to pull the UAV out of the local minima by avoiding the force equilibrium state caused by the obstacles.

The structure of this paper is as follows: The second section covers the design of cooperative consensus control laws based on graph theory. The third section introduces the APF, presenting the modified design method employed in this paper. The fourth section provides the formation model for the swarm system and details the corresponding controllers. The fifth section outlines the process of proving system stability. The sixth section includes the simulation analysis, and the final section concludes the paper.

## 2. Graph Theory-Based Cooperative Formation Control

This section presents the design of a multi-agent formation based on affine formation theory. Firstly, it provides the foundational knowledge of graph theory and the definition of affine. Secondly, it introduces the concepts of stress matrix and universal rigidity, along with the design method for a globally rigid graph. Following this analysis, the nominal formation designed in this paper and the communication topology structure of six UAVs are presented. Finally, a cooperative controller based on consistency theory is developed for the cluster system, enabling formation maintenance and affine transformations among the UAVs.

Graph theory, originally an emerging branch of mathematics, now holds a significant position in modern science. It provides a simple and systematic modeling approach for various fields such as physics, control theory, and social sciences. Many problems can be transformed into graph theory problems and subsequently solved using fundamental graph theory algorithms. In the control of multi-agent formation, the agents' communication relies on the establishment of network topology. From the topological graph, one can intuitively observe the flow of information among various communication nodes.

Modeling is done using graph theory, where vertices represent intelligent agents and edges represent the communication distance between the intelligent agents [26]. The number of vertices and edges in a directed simple graph are determined to be  $n$  and  $m$ , respectively.  $G = (v, \varepsilon)$   $v = \{1, 2, \dots, n\}$ ,  $\varepsilon \subseteq v \times v$  are referred to as the vertex set and the edge set of the graph  $G$ , respectively, where  $|\varepsilon| = m$ . The set of neighboring vertices of vertex  $i$ , represented by  $N_i = \{j \in v : (i, j) \in \varepsilon\}$ , is considered. Therefore,  $(G, p)$  represented a formation and the graph  $G$  where its vertex  $i$  map to  $p_i$ .

An affine transformation may be conceptualized as a variant of linear transformation [27]. Figure 1 illustrates how these transformations manifest through operations like translation, rotation, scaling, shearing, or their combinations [28]. If we have a set of points  $\{p_i\}_{i=1}^n$  in  $R^d$ , we can express the affine span of these points as Equation (1).

$$S = \left\{ \sum_{i=1}^n a_i p_i : a_i \in R, \sum_{i=1}^n a_i = 1 \right\} \tag{1}$$

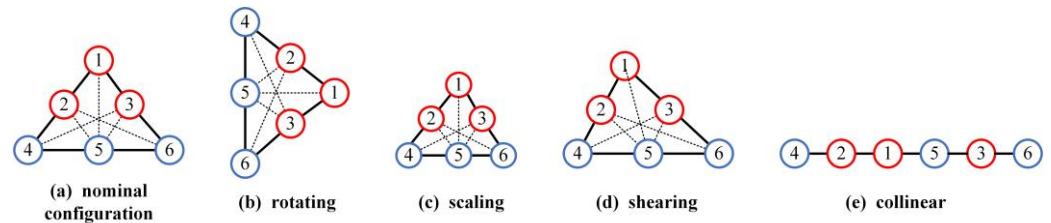


**Figure 1.** Affine transformation types of six UAVs. (The red circle represents the Leader and the blue circle represents the Follower. The numbers inside the circles represent the identification of the UAVs.)

The affine space will be used to describe the interrelations among the individuals in the formation.

The subsequent discussion will introduce Lemma 1, which serves to establish the rank condition for the affine span.

**Lemma 1** (Rank condition for affine span). *The set of points  $\{p_i\}_{i=1}^n$  affinely span  $R^d$  if and only if  $n \geq d + 1$  and  $rank(\bar{P}(p)) = d + 1$ .*

Matrices are mathematical tools used in graph theory analysis. By studying the properties of matrices, the characteristics of the communication topology graph can be obtained. The stress matrix [29] describes the communication topology relationships among UAVs. Utilizing the stress matrix allows not only the description of topological connections between agents but also indicates the strength of these connections and the direction of information flow. Numerical values with positive or negative values indicate attraction or repulsion between UAVs. In the stress matrix, when  $w_{ij} > 0$  is positive, it indicates the presence of an attractive force along edge  $(i, j)$ ; conversely, if  $w_{ij} < 0$  is negative, it suggests the existence of a repulsive force. Vector  $w_{ij}(q_j - q_i)$  represents the force exerted by UAV  $j$  on intelligent agent  $i$  through edge  $(i, j)$ . If formation  $(G, q)$  can meet the following requirements (2):

$$\sum_{j \in N_i} w_{ij}(q_j - q_i) = 0, \forall i \in \{1, \dots, n\} \tag{2}$$

then, it is defined that  $w$  is equilibrium stress of  $(G, q)$ . The rigidity [30] will reveal the uniqueness of the formation structure up to congruence. The generic configuration can be denoted by  $q = [q_1^T, \dots, q_n^T]^T \in R^{nd}$ . A framework  $(G, q)$  refers to a corresponding graph  $G$  with its configuration. A structure  $(G, q)$  is called rigid in  $R^d$  if all the structures  $(G, p)$  equivalent to  $(G, q)$  and sufficiently close to  $(G, q)$  are congruent to  $(G, q)$  in  $R^d$ . If all the structures  $(G, p)$  equivalent to  $(G, q)$  are congruent to  $(G, q)$ , it is called globally rigid in  $R^d$ . What is more, if this congruent relationship holds in any higher-dimensional space  $R^D \supset R^d$ , we say it is universally rigid [31].

According to the requirements of a rigid swarm, Lemma 2 states that the stress matrix should satisfy the following condition [32]:

**Lemma 2** (Generic universal rigidity). *Let  $(G, q)$  be a generic framework on  $n$  vertices in  $R^d, d \leq n - 2$ . Then,  $(G, q)$  is universally rigid if and only if there exists a positive semi-definite stress matrix  $\Omega$  such that its rank is  $n - d - 1$ .*

To simplify collaborative interactions and enhance information transmission efficiency, we employ a Leader–Follower formation control strategy, where the desired formation maneuvers are exclusively communicated to the leaders. We establish the assumption that the initial  $n_l$  agents in the formation are designated as leaders, while the remaining  $n_f = n - n_l$  agents are termed followers. Throughout this article,  $l$  and  $f$  represent the variables for leaders and followers, respectively [33].

**Lemma 3** (Leader selection for affine localizability). *The nominal formation  $(G, r)$  is affinely localizable if and only if  $\{r_i\}_{i \in v_l}$  affinely span  $R^d$ .*

In scenarios where there are precisely  $d + 1$  leaders, for any given leader position  $p_l$ , a solution  $(A, b)$  to Equation (3) always exists. However, when the number of leaders exceeds  $d + 1$ , the positions of the leaders become interdependent. Otherwise, the absence of a solution  $(A, b)$  to Equation (3) is plausible, as the equation constitutes an overdetermined linear system. For the purpose of this paper, three agents are designated as leaders within the formation, identified as Leader 1, 2, and 3.

$$p^*(t) = A(t)r + b(t) \tag{3}$$

Based on the formation dimension and the number of intelligent agents, the maximum number of edges for a formation-based topology according to graph theory is provided. By following the described method, one can calculate the upper limit of the number of connections between formations [34].

**Lemma 4** (The upper bound on the number of sides). *The number of members of the constructed tensegrity framework is bounded from above by*

$$|\epsilon| \leq (d + 1)\left(n - \frac{d + 2}{2}\right)$$

From the above Lemmas 1–4, we can derive the conditions for constructing formation topology. According to the theory mentioned above, a configuration in a two-dimensional plane requires three leaders, giving the design of a formation configuration consisting of the six UAVs (Figure 2).

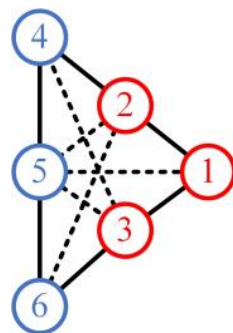


**Figure 2.** Nominal topological connectivity graph.

The UAVs numbered from one to three serve as leaders in the formation, while the remaining UAVs act as followers. Based on the designed formation topology, the adjacency matrix can be obtained [35]. This paper does not present a distinct control law for leaders. It is established that the leader’s position aligns with the expected value in the target configuration, denoted as  $p_l(t) = p_l^*(t)$  for all times. Consequently, our control objective is to guide the followers towards attaining  $p_f(t) \rightarrow p_f^*(t)$ .

This paper designs the following control laws (4) based on consensus theory to achieve a consensus among the swarm of UAVs in the formation. Under the influence of these control laws (4), the UAV swarm not only maintains velocity consensus, but each UAV also remains at its designated position based on the topology.

$$u_{ij} = - \sum_{j \in N_i} w_{ij} [k_p(p_i - p_j) + k_v(v_i - v_j)] \quad (4)$$

where  $w_{ij}$  represents the element of the stress matrix,  $p_i, p_j$  denotes the position of UAVs  $i$  and  $j$ , and  $v_i, v_j$  represents the velocity of the UAVs.  $\dot{v}_j$  is the acceleration of the  $j$ -th UAV. In addition,  $k_p, k_v$  represents the position and velocity gain coefficients between the UAV and its adjacent.

From the above equation, it is evident that the calculation of the control input considers the state variables of neighboring UAVs, such as velocity and position. Therefore, utilizing the foundation of the consistency algorithm and the stress matrix, followers can maintain the designed formation topology during the formation process, preventing collisions. When a UAV deviates from the entire formation, the force exerted by the adjacency matrix between UAVs acts as the attraction, pulling the deviating UAV back into the formation and maintaining the stability of the formation shape.

### 3. Design Improvement of the APF Method

The principle of the APF method proposed by Khatib is to model the environment as a potential field [36]. In this space filled with the potential field, there is a repulsive field around obstacles and an attractive field around the target point [37]. Under the combined influence of attraction and repulsion, the UAV moves towards the target point, and the resultant force generated by the superposition of various potential fields determines the direction of the UAV motion. Compared to other obstacle avoidance algorithms, APF possesses advantages such as lower computational complexity and high real-time performance. However, it also has its own drawbacks, such as issues with local minima and unreachable targets.

#### 3.1. Designing an Improved APF Method

Inaccessibility to the target is a significant drawback of the APF method [38], and this situation may arise in the following scenarios: (1) There are obstacles around the target, and the repulsion force acting on the UAV next to the target is greater than the attraction force. (2) When the attraction force at the current position is greater than the repulsion force, the UAV moves towards the target point. However, in the next moment, the situation is the opposite. This situation can lead to the UAV repeatedly jumping around the current position but never truly approaching the target point.

There has been some research on improving the APF method, as mentioned above. However, the environments considered in these studies are relatively simple, and they do not take into account the scenario of multiple UAV formations. In addressing the issue of an unreachable target, this study innovatively integrates the Leader-Follower formation method into the traditional APF. A repulsive field is established only around obstacles, eliminating the attractive field around the target point. The UAVs' attractive force is generated by the force exerted by the leader on the followers, and its magnitude depends on the designed formation topology. By planning a trajectory in advance that reaches the target point, the leader enables the followers to avoid the issue of target inaccessibility through their guidance. This enhancement provides a more realistic simulation of complex environments. Assuming the environment has multiple obstacles, the definitions for the detection area and collision area (Figure 3) for the  $m$ -th obstacle are in (5) and (6).

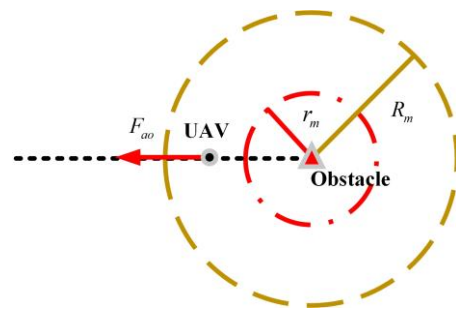


**Figure 3.** Artificial repulsion field detection and collision area map.

The collision region of obstacle  $m$ :

$$\beta_{\text{collision}} \triangleq \{x | \|x - x_{o_m}\| \leq r_m\} \tag{5}$$

The detection region of obstacle  $m$ :

$$\beta_{\text{detection}} \triangleq \{x | r_m < \|x - x_{o_m}\| \leq R_m\} \tag{6}$$

Effectively defining the detection and collision zones for UAVs simplifies the computations by excluding repulsive forces when the UAVs are distant from obstacles. The improved repulsive field function (7) is designed as

$$E_{ao_m}(x) = \begin{cases} \beta_1 \left( \frac{\chi(x, x_{o_m})}{R_m^2} - \frac{2 \ln \chi(x, x_{o_m})}{R_m} - \frac{1}{\chi(x, x_{o_m})} \right) & \chi(x, x_{o_m}) \in \beta_{\text{collision}} \\ 0 & \chi(x, x_{o_m}) \notin \beta_{\text{collision}} \end{cases} \tag{7}$$

where  $E_{ao_m}$  represents the repulsive field function, and  $x_{o_m}$  and  $R_m$  represent the center position and the effective range of the force of obstacle  $m$ , respectively.  $\beta_1$  is the repulsion gain coefficient.  $\chi(x, x_{o_m}) = \|x - x_{o_m}\|$  is the distance from the UAV to the center of the obstacle.

The negative gradient of the modified repulsive function (8) is calculated, resulting in the following obstacle repulsive force:

$$F_{ao_m}(x) = -\nabla E_{ao_m}(x) = \begin{cases} \beta_1 \left( \frac{1}{\chi(x, x_{o_m})} - \frac{1}{R} \right)^2 & \chi(x, x_{o_m}) \in \beta_{\text{collision}} \\ 0 & \chi(x, x_{o_m}) \notin \beta_{\text{collision}} \end{cases} \tag{8}$$

In the equation,  $F_{ao_m}$  is the force exerted on the agent due to repulsion. According to the improved APF, it can be observed that, when calculating the repulsive force of obstacles on drones, the distance between the UAV and the center of the obstacle  $\chi(x, x_{o_m})$  is first calculated. Since various obstacles may be present in the environment, the repulsive force acting on an individual is the sum of the repulsive forces, as in (9), generated by all obstacles.

$$F_{ao_i} = \sum_{m=1}^n F_{ao_m} \tag{9}$$

In Equation (9),  $F_{ao_i}$  represents the sum of the repulsive forces exerted by multiple obstacles on the  $i$ -th intelligent agent.

Based on the improved APF mentioned above, with the guidance from the leader to the followers, the attractive force field is omitted, thus avoiding the problem of unreachable targets. The action range of each field is clearly defined, continuously monitored during the formation process. When encountering obstacles, the obstacle avoidance mode is triggered, generating corresponding repulsive forces to assist the UAV swarm.

### 3.2. Addressing the Issue of Local Extrema in the APF Method

When facing obstacles with special shapes or specific combinations, UAV systems may encounter local extremum points. In other words, the resultant force of the repulsive forces acting on the UAV becomes zero, leading to a halt in motion [39]. The three common situations where the UAV can be trapped in extremum points are illustrated in the following Figure 4. Some scholars have attempted to introduce perturbations. However, extensive experiments indicate that perturbation-based approaches suffer from low reliability. The second approach involves proactively abandoning the pursuit of the target point, designing new subgoals, and altering its gravitational source. Nonetheless, there is a possibility that the gravitational effect of the next subgoal point may not show a significant improvement or that there is no defined next subgoal point. In such cases, our method becomes impractical.

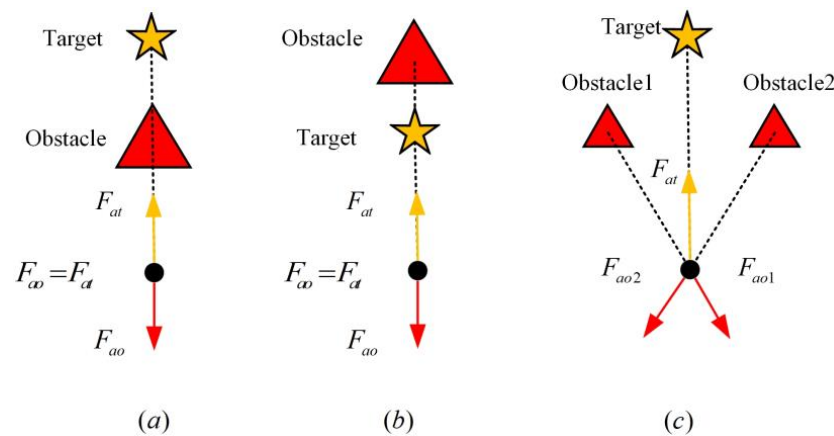


**Figure 4.** The three cases of local extremum points. ((a) and (b) are the cases where the obstacle and the target point are collinear, and the attraction and repulsion forces are equal in magnitude and opposite in direction. (c) is the case where the sum of the repulsive forces generated by the two obstacles is equal to the attraction of the target point).

To address the potential issues described earlier, our study introduces a “rotational force”. By adjusting the force direction, the agent’s movement deviates. The rotational force’s magnitude is proportional to the repulsive force from the nearest obstacle to the UAV, aligning with the obstacle’s normal direction. The specific direction of the rotational force depends on the target point’s position relative to the obstacle. For example, if the target point is to the right of the obstacle, the rotational force will direct to the right. The details are illustrated in Figure 5.

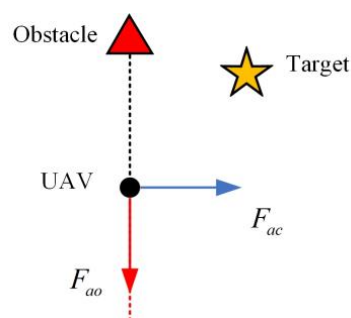


**Figure 5.** Rotational force diagram.

The rotational force enables the UAV to move parallel to the obstacles, resulting in a smoother trajectory. This is because avoiding local extremum points does not necessarily require moving away from them; instead, it involves making local adjustments to the force direction. Therefore, introducing the rotational force does not impact the overall stability of the swarm. The magnitude of the force ( $F_{ac_m}$ ) is equal to the product of the repulsive

force magnitude and the gain coefficient. The specific formula for the calculation is as Equation (10).

$$F_{ac_m}(x) = \begin{cases} \zeta_1 F_{aom}(x), & \chi(x, x_{om}) \leq \eta_1 R \\ 0, & \chi(x, x_{om}) > \eta_1 R \end{cases} \quad (10)$$

In the equation,  $\zeta_1$  represents the gain coefficient, and  $\eta_1$  is a parameter related to the effective range of the rotational force. The effective range parameter indicates that the rotational force is only active when the UAV is at a certain distance from obstacles or when the net external force is zero. In all other situations, the rotational force is set to zero. This design allows the UAV to escape from the local extremum point.

#### 4. Control of UAV Swarm Formation Based on the Improved APF Method

The position deviation based on the consensus protocol can guide all UAVs to converge to the desired topological positions while ensuring a safe distance between them. With the introduction of APF [40], utilizing the repulsive forces generated by obstacles on UAVs, the coordinated avoidance control objective can be achieved through the multiple repulsive potential fields. The introduction of rotational force allows the UAV to promptly escape extremum points and reach the target point.

Taking a single UAV as an example, to maintain the formation, the UAV adjusts its attractive or repulsive force concerning the real-time information and the configuration. In the event of a UAV deviating from the formation, the inter-agent attractive force is utilized to pull it back into the formation. In the case of two UAVs being too close, repulsive forces are applied between them, guiding each UAV to its desired position under this force. When facing obstacles, the established APF comes into play [41]. The control diagram for an individual UAV is depicted below (Figure 6).

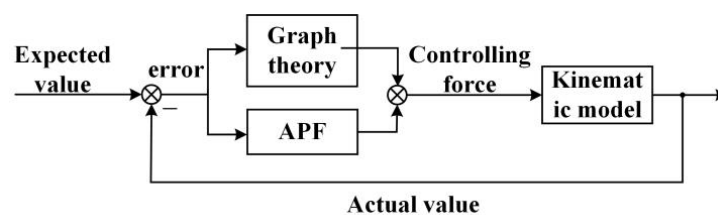


Figure 6. Control block diagram of a single UAV.

Building upon the aforementioned single UAV control, the focus shifts to achieving overall formation control for a swarm. Employing a Leader–Follower formation approach, the design incorporates knowledge from graph theory to establish the formation topology. Building on the principles of consistency, the control system coordinates the relative positions and velocities of the leader and followers. As these variables gradually converge, maintaining stability in the formation, the ultimate goal of formation control is achieved.

The second-order continuous system model for formation control is represented by (11).

$$\begin{cases} \dot{x}_i = v_i \\ \dot{v}_i = u_i \end{cases} \quad (11)$$

In Equation (11),  $x_i, v_i, u_i \in R_n$  represent the position, velocity, and applied control force of the UAV, while  $n$  denotes the dimensionality of the state variables. The role of the leading UAV is crucial for the overall formation, and in this study, it is assumed that the leader has been well-planned, with a safe path to reach the target point. Followers only need to track the leader’s trajectory to maintain formation stability. Throughout the formation process, the repulsive force generated proves effective in avoiding obstacles. In summary, considering the combined effect of various forces, the resultant force experienced by the UAV in the swarm formation is (12).

$$F_{all} = F_{ij} + \sum_{m=1}^M F_{ao_m} + F_{ac_m} \tag{12}$$

$F_{all}$  represents the total resultant force experienced by the UAV, and  $F_{ij}$  represents the interaction forces designed based on consistency theory, as expressed in Equation (4).  $\sum_{m=1}^M F_{ao_m}$  denotes the resultant force from the repulsive effects generated by multiple obstacles, with the repulsive force expression provided in Equation (8).  $F_{ac_m}$  stands for the rotational force utilized by the UAV after force equilibrium to escape extremum points, with its expression outlined in Equation (10).

Therefore, based on the resultant force experienced by the UAV, the velocity and position update states for each UAV can be obtained through the following (13)–(15) calculations.

$$a_{t+1} = \frac{F_{all}}{m_i} \tag{13}$$

$$v_{t+1} = v_t + a_{t+1} \times \Delta_t \tag{14}$$

$$p_{t+1} = p_t + v_{t+1} \times \Delta_t \tag{15}$$

In Equations (13)–(15),  $m_i$  represents the total mass of UAV  $i$ ,  $a_{t+1}$  is the acceleration at time  $t + 1$ ,  $v_{t+1}, p_{t+1}$  represents the velocity and position at time  $t + 1$ ,  $v_t, p_t$  represents the velocity and position at time  $t$ , and  $\Delta_t$  is the time interval for state updates.

The computational process of the swarm formation control algorithm based on the enhanced APF is as follows:

1. **Initialization Phase:** Initialization of the number and spacing of UAVs in the formation, positions of obstacles, and the range of repulsive forces; computation of the adjacency matrix and stress matrix for configuration topology; initialization of the parameters for the enhanced APF and consistency algorithm.
2. **Generate Interaction Force:** Calculate the control forces needed to maintain the formation configuration among UAVs based on the formation structure, stress matrix, and the positions and velocities of neighboring UAVs.
3. **Computation and Detection:** Compute the distances between each UAV and various obstacles and determine whether obstacle avoidance is necessary. Calculate the repulsive forces acting on each UAV based on the designed potential field.
4. **Force Summation:** Following steps 2 and 3, obtain the resultant force acting on the UAV and assess whether the UAV is trapped in a local extremum. If so, introduce rotational force and update the net external force.
5. **Update States:** Update the time, and according to the swarm model, calculate the positions, velocities, and accelerations of each UAV for the next time step.
6. **Evaluation Outcomes:** Check whether the UAVs have reached the target point. If they have, the formation task concludes. If not, return to step 2.

Draw the flowchart based on the steps of the cluster formation operation.

### 5. Stability Verification of the UAV Swarm System

Divide the UAV cluster into leaders and followers, assuming that the leader has already planned a path to reach the target safely and achieved global stability. Next, we only need to demonstrate that, under the control laws (16) designed in this paper, the followers can maintain global stability [42]. Therefore, the controls discussed below are specifically related to the follower UAVs (Figure 7).

$$u_i = - \sum_{j \in N_i} w_{ij} [k_p(\hat{x}_i - \hat{x}_j) + k_v(\hat{v}_i - \hat{v}_j)] + F_i^{APF} \tag{16}$$

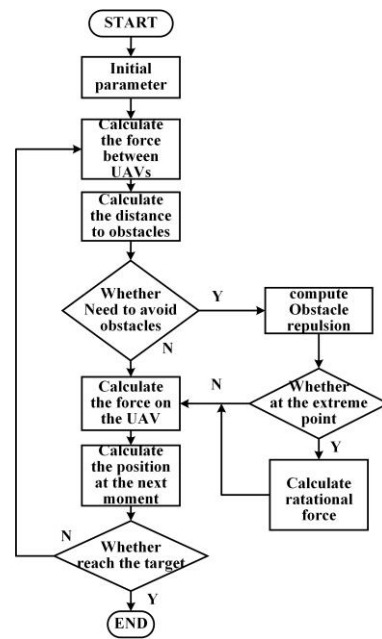


**Figure 7.** Flow chart of the formation and obstacle avoidance algorithm based on the improved APF method.

$F_i^{APF}$  represents the total APF forces acting on the  $i$ -th follower, and  $u_i$  denotes the control force of the following UAV.

Assuming vectors  $\hat{x}_i = x_i - x_i'$  and  $\hat{v}_i = v_i - v_i'$ , where  $x_i'$  and  $v_i'$  are, respectively, the desired position and desired velocity of the UAV.  $\hat{x} = [\hat{x}_1^T \ \hat{x}_2^T \ \dots \ \hat{x}_n^T]^T \in \mathbb{R}^{n \times 2}$ ,  $[\hat{v} = \hat{v}_1^T \ \hat{v}_2^T \ \dots \ \hat{v}_n^T]^T \in \mathbb{R}^{n \times 2}$ , and  $F^{APF} = [F_1^T \ F_2^T \ \dots \ F_n^T]^T$ . Therefore, the control inputs of the entire UAV formation system can be rewritten as (17):

$$\dot{v} = -k_p \bar{\Omega} \hat{x} - k_v \bar{\Omega} \hat{v} + F^{APF} \tag{17}$$

Assume  $x' = [(x_1')^T \ (x_2')^T \ \dots \ (x_n')^T]^T \in \mathbb{R}^{n \times 2}$ ,  $v' = [(v_1')^T \ (v_2')^T \ \dots \ (v_n')^T]^T$ .

Separate the real-time state values of each from the desired values. Then, we can achieve Equation (18).

$$\dot{v} = -k_p \bar{\Omega} x - k_v \bar{\Omega} v + k_p \bar{\Omega} x' + k_v \bar{\Omega} v' + F^{APF} \tag{18}$$

Thus, the kinematic model of the UAV formation system can be described as (19).

$$\begin{bmatrix} \dot{x} \\ \dot{v} \end{bmatrix} = \begin{bmatrix} \mathbf{0}_n & \mathbf{I}_n \\ -k_p \bar{\Omega} & -k_v \bar{\Omega} \end{bmatrix} \begin{bmatrix} x \\ v \end{bmatrix} + \begin{bmatrix} \mathbf{0}_n \\ F^{APF} \end{bmatrix} + \begin{bmatrix} \mathbf{0}_n & \mathbf{0}_n \\ k_p \bar{\Omega} & k_v \bar{\Omega} \end{bmatrix} \begin{bmatrix} x' \\ v' \end{bmatrix} \tag{19}$$

First, consider the stability of the following homogeneous Equation (20):

$$\begin{bmatrix} \dot{x} \\ \dot{v} \end{bmatrix} = \begin{bmatrix} \mathbf{0}_n & \mathbf{I}_n \\ -k_p \bar{\Omega} & -k_v \bar{\Omega} \end{bmatrix} \begin{bmatrix} x \\ v \end{bmatrix} + \begin{bmatrix} \mathbf{0}_n \\ F^{APF} \end{bmatrix} \tag{20}$$

Use Equation (21) to define the Lyapunov function [43].

$$V(x, v) = \frac{1}{2} v^T v + \frac{1}{2} k_p x^T \bar{\Omega} x + U(x) \tag{21}$$

where  $U(x)$  represents the total potential energy of the follower UAVs under the APF. Taking its derivative yields the potential field force (22) acting on the UAVs.

$$\dot{U}(x) = F^{APF} = \dot{v} + k_p \bar{\Omega} \hat{x} + k_v \bar{\Omega} \hat{v} \quad (22)$$

Taking the derivative of the Lyapunov function yields Equation (23):

$$\begin{aligned} \dot{V}(v) &= v^T \dot{v} + k_p v^T \bar{\Omega} x + v^T (-\nabla_x U) = v^T (-\nabla_x U + \dot{v} + k_p \bar{\Omega} x) \\ &= v^T (-(\dot{v} + k_p \bar{\Omega} x + k_v \bar{\Omega} v) + \dot{v} + k_p \bar{\Omega} x) = -k_v v^T \bar{\Omega} v \end{aligned} \quad (23)$$

Due to the positive semi-definiteness of matrix  $\bar{\Omega}$ , it follows that  $\dot{V}(v) \leq 0$ . Therefore, when  $t \rightarrow \infty$ ,  $V(x, v)$  monotonically decreases. Define set  $L_V(c) = \{(x, v) | V(x, v) \leq c\}$  as a bounded set in this case. If the initial state of the UAV is  $(x(0), v(0)) \in L_V(c)$ , then  $V(x(t), v(t)) \leq c$  holds for all times  $t$ , and  $L_V(c)$  is an invariant set. For  $\forall (x, v) \in L_V(c)$ ,  $\dot{V}(v)$  is a semi-negative definite. According to LaSalle's invariance principle, if  $t \rightarrow \infty$ , the UAV system will converge into the largest invariant set of  $L_V(c)$ , denoted as  $\Omega = \{v\} \dot{V}(v)$ . Therefore, solving for  $\dot{V}(v) = 0$  yields  $v_1 = v_2 = v_1 = \dots = v_n = 0$ . At the same time, the total potential energy of the UAV formation system is represented by  $U(x) \geq 0$ , and the potential field is zero only when the system is free from obstacle interference and internally stable.

Next, we solve for the particular solution of the nonhomogeneous equation. Assuming that, when the UAV system is only influenced by the potential field forces and not by inter-agent interactions, at this point, the system achieves consensus, which leads to the solution  $[x, v]^T = [x', v']^T$  when substituted. The general solution of the nonhomogeneous equation is the sum of its homogeneous equation general solution and its particular solution. Therefore, when  $t \rightarrow \infty$ , the solution of Equation (20) converges gradually to  $[x', v']^T$ .

In summary: when gains  $k_p$  and  $k_v$  are positive, all state values of the UAVs within the formation will tend to become the largest invariant set. All UAVs' state values can converge into the desired position and velocity, achieving consensus. The inter-agent spacing can converge into the optimal distance and asymptotically maintain stability, forming a stable formation.

## 6. Simulation Analysis of Drone Swarm on Multiple Platforms

To validate the effectiveness of the proposed strategy, simulations and real-world experiments were conducted during the UAV formation flight phase. The simulation involved validation using both the MATLAB (R2022b) platform [44] and the ROS (Robot Operating System) [45]. The corresponding swarm formation results were analyzed separately, and comparisons were made with other algorithms. Finally, the feasibility of the proposed method was reaffirmed through experiments on quadcopter UAVs.

### 6.1. MATLAB Simulation

Simulation verification of the formation strategy for the six UAVs in a two-dimensional environment was conducted. The results included the overall formation route map, velocity curves, heading angles, inter-UAV distances, and the minimum distance graph. This illustrates that the strategy is capable of successful obstacle avoidance and reaching the target point in the presence of multiple obstacles.

#### 6.1.1. Formation Control Simulation Analysis

The simulation scenario involves six UAVs performing multiple obstacle avoidance maneuvers and the overall formation turns while moving forward. The six circles represent the UAVs, with the red circles numbered 1–3 serving as leaders and the blue circles 4–6 as followers. The simulation parameters are as follows:

Based on the topology configuration of the six UAVs designed in Figure 2 combined with the adjacency matrix, the stress matrix can be calculated as shown (Table 1).

**Table 1.** Stress matrix  $w_{ij}$  of the six UAVs' formation topology.

| $j \setminus i$ | 1       | 2       | 3       | 4       | 5       | 6       |
|-----------------|---------|---------|---------|---------|---------|---------|
| 1               | -0.3992 | 0.3922  | 0.3922  | 0       | -0.3922 | 0       |
| 2               | 0.3922  | -0.7845 | 0       | 0.1961  | 0.3922  | -0.1961 |
| 3               | 0.3922  | 0       | -0.7845 | -0.1961 | 0.3922  | 0.1961  |
| 4               | 0       | 0.1961  | -0.1961 | -0.1961 | 0.1961  | 0       |
| 5               | -0.3922 | 0.3922  | 0.3922  | 0.1961  | -0.7845 | 0.1961  |
| 6               | 0       | -0.1961 | 0.1961  | 0       | 0.1961  | -0.1961 |

Assuming the UAVs initiate the formation from randomly chosen initial positions, they quickly shape the designed triangular formation in the early stages. During the progress, they repeatedly avoid obstacles and then maintain a straight line formation for turning, ultimately reaching the endpoint. The initial positions are shown in Table 2.

**Table 2.** Different starting positions for the UAVs.

| Drone Number | Drone Role | Initial Position |
|--------------|------------|------------------|
| 1            | Leader     | (200, 0)         |
| 2            | Leader     | (-900, -200)     |
| 3            | Leader     | (200, -500)      |
| 4            | Follower   | (-100, -1500)    |
| 5            | Follower   | (800, -1250)     |
| 6            | Follower   | (1000, -750)     |

In the simulation, three cylindrical obstacles are introduced to simulate a complex formation environment. Table 3 provides the positional coordinates of the three obstacles. The detailed simulation parameter information for the formation control is presented in Table 4.

**Table 3.** Obstacle position coordinates.

| Obstacle Number | Position Coordinate | Sphere of Influence $R_m$ |
|-----------------|---------------------|---------------------------|
| 1               | (700, 2000)         | 300 m                     |
| 2               | (-250, 3600)        | 250 m                     |
| 3               | (650, 5200)         | 250 m                     |

**Table 4.** Simulation parameter table.

| Parameter                                     | Value  |
|---|--------|
| $k_p$   | 0.5    |
| $k_v$   | 2      |
| $v_{leader}$ (Speed of a leader)              | 45 m/s |
| $v_{min}$ (Minimum speed of the follower)     | 8 m/s  |
| $v_{max}$ (The maximum speed of the follower) | 62 m/s |
| $r_j$   | 200 m  |
| $R_j$   | 400 m  |
| $\beta_1$                                     | 30     |
| $\zeta_1$                                     | 0.05   |

Based on the known formation reconstruction and obstacle avoidance parameters mentioned above, the trajectory routes of the six drones are shown in the diagram below. The drone swarm rapidly forms a triangular configuration from random initial positions and then, in three separate instances, maneuvers around cylindrical obstacles. At time  $t = 176$  s, the cluster transitions from a triangular configuration to a straight line formation. At time  $t = 230$  s, the six drones collectively form a half-circle formation, ultimately reaching the target point in an evenly spaced straight line configuration (Figure 8).

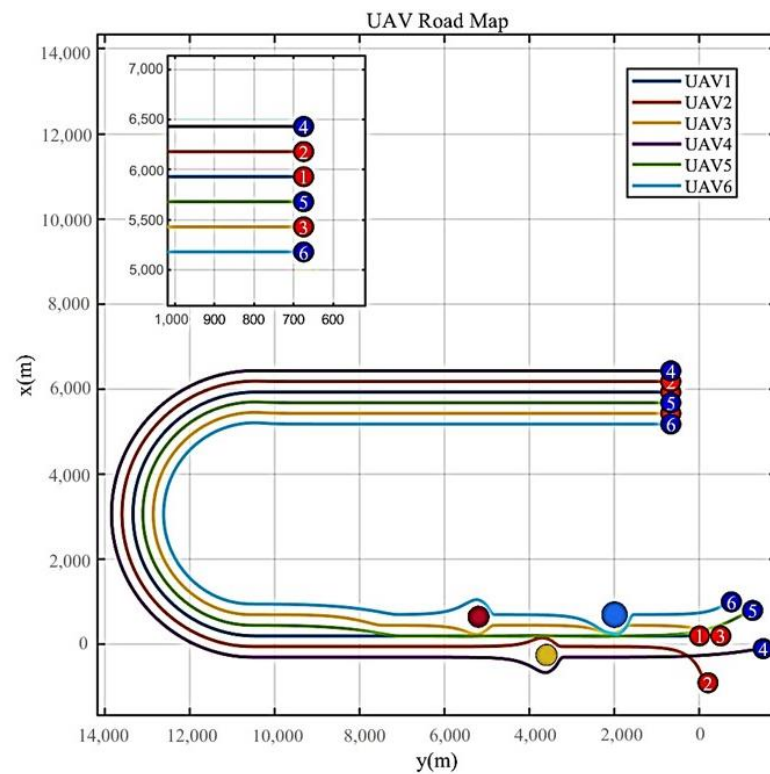


**Figure 8.** Cluster formation overall trajectory roadmap. (The red, yellow and blue circles represent three different obstacles in the path)

The speed curves under different control strategies are presented in Figure 9. Figure 9a depicts the formation and obstacle avoidance speed profile achieved by combining the APF and PI controller. Figure 9b illustrates the formation strategy adopted in this paper. It can be observed that, when encountering various obstacles in the environment, the traditional APF approach leads to significant oscillations and shaking, with a large overshoot. The speed fluctuates rapidly within a short period, ranging from 10 m/s to 59 m/s. However, with the control strategy proposed in this paper, the drone cluster exhibits smoother motion when encountering obstacles, with minimal overshoot, swiftly navigating around obstacles. At time T1, the formation transitions from a triangular configuration to a single file pattern, resulting in speed changes for the other drones as they accelerate to align with the position of drone number one on the same horizontal line. At time T2, the cluster collectively forms a circular pattern. Due to the distinction between the inner and outer circles, the sixth drone in the innermost circle slows down due to the shorter distance traveled, while the fourth drone, covering the maximum circular path, accelerates to maintain the formation. Ultimately, the cluster maintains a velocity of 45 m/s towards the target point.

Figure 10a illustrates the variation in distances between each UAV and UAV 1 under the influence of formation control. The final steady-state distances between the UAVs are related to the designed initial formation spacing, denoted as  $l = 250$  m. After experiencing fluctuations through three obstacles, the distances between UAVs 2 and 5 from UAV 1 are both 250 m, between UAVs 3 and 4 from UAV 1 are 500 m, and UAV 6 is the farthest, with a distance of 750 m. Figure 10b represents the minimum distances between the UAVs. At the initial position, the minimum distance between the UAVs is 500 m. By the end of the motion, the formation has been achieved and maintained, with the minimum inter-UAV distance stabilizing at 250 m. The spacing diagram presented above indicates that there were no collisions between the unmanned aerial vehicles.

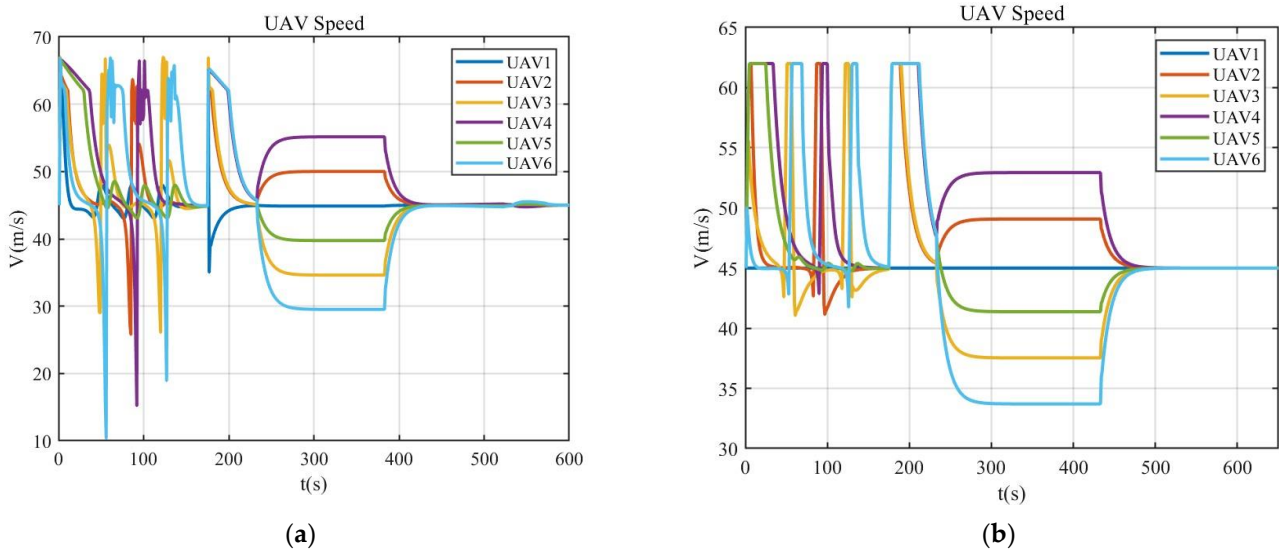


**Figure 9.** UAV speed curve. (a) Using PI and APF control for the UAV cluster speed. (b) The control strategy proposed in this article.

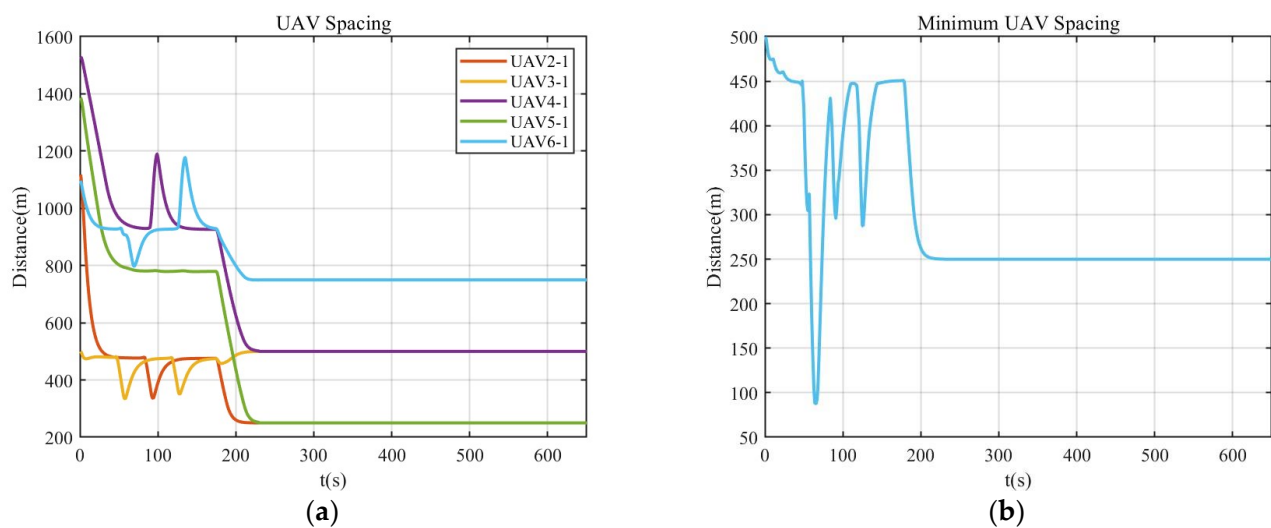


**Figure 10.** Drone spacing diagram. (a) The distance between each UAV and UAV 1. (b) Minimum distance between the drones and each other.

### 6.1.2. Local Extremum Issues in APF

To address the local minima problem in the APF, this paper introduces a rotational force. When a UAV becomes trapped in a local minimum and cannot escape, an external force is applied to disrupt its force equilibrium. Figure 11 compares different methods. Under PI control, in case 1, the UAV circumvents obstacles from the outer circle, which increases the total path length and extends the time to reach the destination. Case 2 represents the situation without rotational force, causing the UAV to become stuck in local minima when facing multiple obstacles. In case 3, the method designed in this paper is employed. Even when trapped in a local minimum, the UAV can still change its overall force with the help of the rotational force. Compared to PI control, the proposed method offers a shorter formation path, potentially saving more fuel and time.



The following depicts the transition of four UAVs from a triangular configuration to a line in Gazebo. The UAVs fly at an altitude of 2 m, with an overhead view at an 45° angle. The shadows of the UAVs' flights are projected onto the grid (Figure 13). The images in the first row, from left to right, show the triangular configuration, the transition from triangular to a line, and the line. Below each image, there are corresponding  $x, y$ -axis coordinate changes for the four UAVs in different states. In Figure 14, it can be observed that, during the transition, the  $x$ -axis position of UAV 2 changes from 2 m to 0. In Figure 15, after the transformation, the  $y$ -axis coordinates show the four UAVs with a spacing of 2 m. This further validates the effectiveness of the formation control proposed in this paper within the ROS.

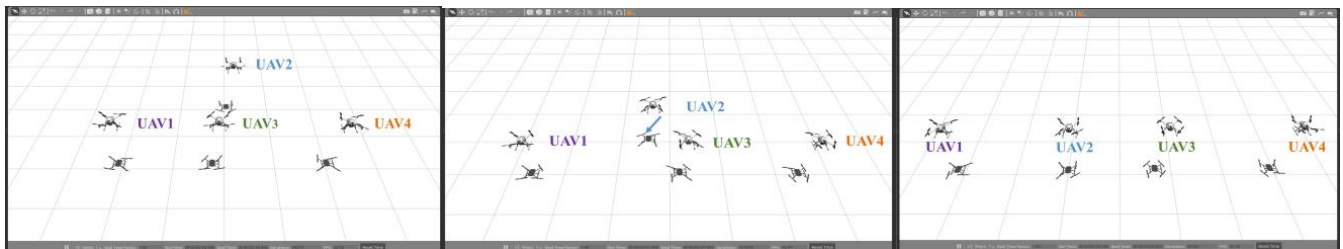


Figure 13. Four UAVs went from a triangle to line.

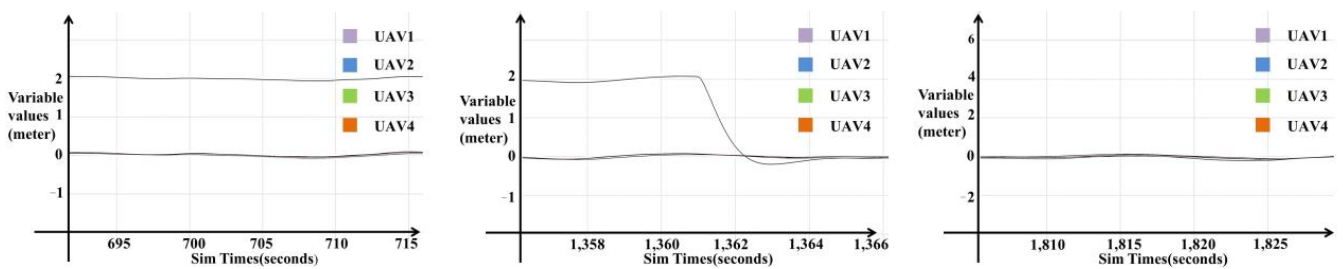


Figure 14. The change in the X-axis coordinates from a triangular configuration to one line configuration.

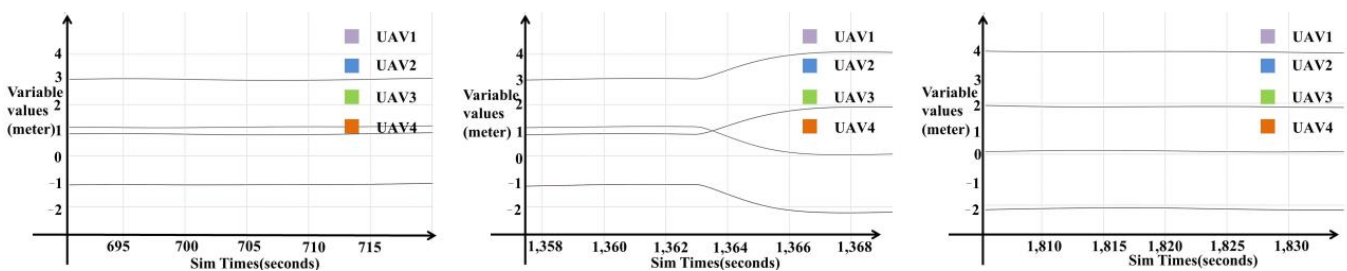


Figure 15. The change in the Y-axis coordinates from a triangular configuration to one line configuration.

### 6.3. Formation Transformation of Quadcopter UAV Swarm

This paper conducted another validation on actual UAVs. Figure 16 shows a graph of four quadcopter UAVs at their initial positions, labeled as UAV 1–4. Figure 17 illustrates the trajectory of the drones as seen from the QGC (QGroundControl) interface. In Figure 17b, after takeoff from the initial point, UAV 3 moves forward while the other drones maintain the formation, forming a triangular pattern. In Figure 17c, the route map depicts the transition of the four drones from triangular to a line. Except for UAV 3, all the other UAVs start flying from the initial point towards positions perpendicular to UAV 3.

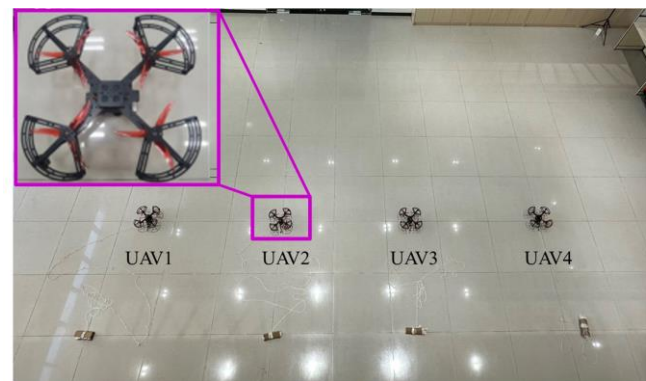


Figure 16. UAV real flight experiment initial position map.

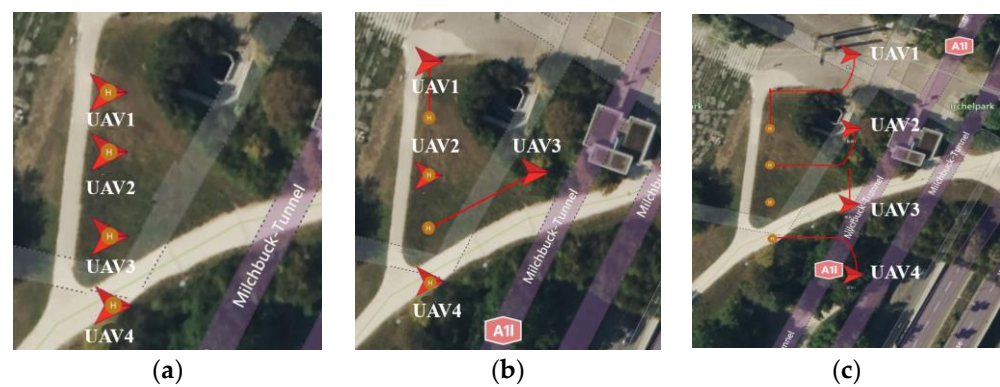


Figure 17. Formation changes of the UAVs in QGC with a real-time route map. (a) The initial positions of the four UAVs in real flight. (b) Formation changes of the four UAVs to a triangle. (c) Formation changes from a triangle to a line.

## 7. Conclusions

This paper integrates a variety of formation methods and successfully addresses the challenges of cooperative formation and obstacle avoidance in UAV swarms. The formation topology is designed by graph theory, while a collision between UAVs is effectively prevented through the stress matrix. The APF approach enables drones to navigate safely in environments with obstacles. The Leader–Follower method reduces the dependence on the gravity of the target point, thus avoiding the unreachable problem. Additionally, rotational forces aid in preventing swarms from becoming trapped in local minimums. By combining these various approaches, the UAV formation achieves its target point without any physical collisions.

The algorithm presented in this paper is successfully simulated and verified using MATLAB(R2022b), ROS (Melodic), and physical machines, thereby demonstrating the feasibility and stability of the proposed strategy. In comparison to the traditional APF method, our algorithm exhibits smoother and faster obstacle traversal with reduced overshoot, demonstrating enhanced robustness in navigating around obstacles.

In the future, we can avoid obstacles in situations where there are multiple types and dynamic obstacles. Additionally, we can explore more challenging task scenarios, such as UAV communication failure, information transmission delay, and variable topological configurations.

**Author Contributions:** Writing—original draft, Y.Z.; methodology, M.C.; project administration, M.C.; writing—review and editing, Y.Z. and C.C.; supervision, J.C.; funding acquisition, J.C. and C.C.; validation, Z.Z.; formal analysis, Z.Z.; software, X.D. All authors have read and agreed to the published version of the manuscript.

**Funding:** This work was supported in part by the National Natural Science Foundation (NO:52275113) and the 2023 Shanghai Excellent Academic Leader Program (23XD1403800).

**Data Availability Statement:** Data are contained within the article.

**Acknowledgments:** We thank all the scientists and principal researchers who prepared and provided the research data. We would also like to thank our colleagues from the College of Astronautics, who provided profound insights and expertise to our research.

**Conflicts of Interest:** The authors declare no conflicts of interest.

## References

1. Hu, J.; Sun, X.; He, L. Time-Varying Formation Tracking for Multiple UAVs with Nonholonomic Constraints and Input Quantization via Adaptive Backstepping Control. *Int. J. Aeronaut. Space Sci.* **2019**, *20*, 710–721. [[CrossRef](#)]
2. Wang, J.; Leone, R.D.; Fu, S.; Xia, J.; Qiao, L. Event-Triggered Control Design for Networked Evolutionary Games with Time-Invariant Delay in Strategies. *Int. J. Syst. Sci.* **2021**, *52*, 493–504. [[CrossRef](#)]
3. Chen, J.; Tan, C.; Mo, R.; Zhang, H.; Cai, G.; Li, H. Research on path planning of three-neighbor search A\* algorithm combined with artificial potential field. *Int. J. Adv. Robot. Syst.* **2021**, *18*, 17298814211026449. [[CrossRef](#)]
4. Wang, J.; Gu, W.; Dou, L. Leader-Follower Formation Control for Multiple UAVs with Trajectory Tracking Design. *Acta Aeronaut. Astronaut. Sin.* **2020**, *41*, 88–98.
5. Lee, G.; Chwa, D. Decentralized Behavior-based Formation Control of Multiple Robots Considering Obstacle Avoidance. *Intell. Serv. Robot.* **2018**, *11*, 127–138. [[CrossRef](#)]
6. Zhen, Q.; Wan, L.; Li, Y. Formation Control of a Multi-AUVs System Based on Virtual Structure and Artificial Potential Field on SE(3). *Ocean Eng.* **2022**, *253*, 111148.1–111148.12. [[CrossRef](#)]
7. Pan, W.; Jiang, D.; Pang, Y.; Li, Y. A Multi-AUV Formation Algorithm Combining Artificial Potential Field and Virtual Structure. *Acta Armamentarii* **2017**, *38*, 326–334.
8. Li, J.; Ji, L.; Li, H. Optimal Consensus Control for Unknown Second-Order Multi-Agent Systems: Using Model-Free Reinforcement Learning Method. *Appl. Math. Comput.* **2021**, *410*, 126451. [[CrossRef](#)]
9. Wang, C.; Liu, C.L.; Liu, S. Robust Fixed-Time Connectivity-Preserving Consensus for Second-Order Multi-Agent Systems with External Disturbances. *IET Control Theory Appl.* **2020**, *14*, 2674–2681. [[CrossRef](#)]
10. Li, W.; Sun, J.; Chen, W. Real-Time Obstacle Avoidance Algorithm for Robots Based on BP Neural Network. *Chin. J. Sci. Instrum.* **2019**, *40*, 204–211.
11. Surname, G.N.; Huang, J.; Wu, S.; Fan, R. Obstacle Avoidance Algorithm of Simulation Robotic Fish Based on Ant Colony Algorithm. In Proceedings of the 2020 Chinese Automation Congress (CAC), Shanghai, China, 6–8 November 2020; pp. 3461–3464.
12. Ning, W.; Dai, J.; Jin, Y.; Li, Y.; Lu, L. Multi-UAV Trajectory Planning Simulation Based on Adaptive Extended Potential Field. *J. Syst. Simul.* **2021**, *33*, 2147–2156.
13. Zhao, R.; Lee, H.K. Fuzzy-Based Path Planning for Multiple Mobile Robots in Unknown Dynamic Environment. *J. Electr. Eng. Technol.* **2017**, *12*, 918–925. [[CrossRef](#)]
14. Xia, Q.S.; Tang, Q.H.; Zhang, L.P. Cooperative Path Planning and Operation Collision Avoidance for Multiple Storage Robots. *Inf. Control* **2019**, *48*, 22–28+34.
15. Wang, Z.; Li, M.; Dou, L.; Li, Y.; Zhao, Q.; Li, J. A Novel Multi-objective Artificial Bee Colony Algorithm for Multi-robot Path Planning. In Proceedings of the IEEE International Conference on Information & Automation, Lijiang, China, 8–10 August 2015; IEEE: Piscataway, NJ, USA, 2015.
16. Matoui, F.; Boussaid, B.; Metoui, B.; Abdelkrim, M.N. Contribution to the Path Planning of a Multi-Robot System: Centralized Architecture. *Intell. Serv. Robot.* **2020**, *13*, 147–158. [[CrossRef](#)]
17. Trujillo, J.-C.; Munguia, R.; Guerra, E.; Grau, A. Cooperative Monocular-Based SLAM for Multi-UAV Systems in GPS-Denied Environments. *Sensors* **2018**, *18*, 1351. [[CrossRef](#)] [[PubMed](#)]
18. Zhang, L.; Mou, J.; Chen, P.; Li, M. Path Planning for Autonomous Ships: A Hybrid Approach Based on Improved APF and Modified VO Methods. *J. Mar. Sci. Eng.* **2021**, *9*, 761. [[CrossRef](#)]
19. Wang, J.; Ding, X.; Wang, C.; Liang, L.; Hu, H. Affine Formation Control for Multi-Agent Systems with Prescribed Convergence Time. *J. Frankl. Inst.* **2021**, *358*, 7055–7072. [[CrossRef](#)]
20. Cao, Y.; Sun, Y. Necessary and Sufficient Conditions for Consensus of Third-Order Discrete-Time Multi-Agent Systems in Directed Networks. *J. Appl. Math. Comput.* **2018**, *57*, 199–210. [[CrossRef](#)]
21. Ma, X.; Mei, H. Mobile Robot Global Path Planning Based on Improved Ant Colony System Algorithm with Potential Field. *J. Mech. Eng.* **2021**, *57*, 19–27.
22. Zhang, J.; Yan, J.; Zhang, P. Fixed-Wing UAV Formation Control Design with Collision Avoidance Based on an Improved Artificial Potential Field. *IEEE Access* **2018**, *6*, 78342–78351. [[CrossRef](#)]
23. Qi, B. Research on UAV Formation Control Technology. Master's Thesis, Changchun University of Science and Technology, Changchun, China, 2022.

24. Zhang, Q.; Chen, B.; Liu, X.; Liu, X.; Yang, H. Ant Colony Optimization with Improved Potential Field Heuristic for Robot Path Planning. *Trans. Chin. Soc. Agric. Mach.* **2019**, *50*, 23–32.
25. Chen, X.; Liu, K.W.; Mao, H.L. Trajectory Planning of Unmanned Aerial Vehicles Based on APF-RRT Algorithm. *Electron. Opt. Control* **2022**, *5*, 17–22.
26. Han, L.; Dong, X.; Li, Q.; Ren, Z. Formation-containment Control for Second-order Multi-agent Systems with Time-varying Delays. *Neurocomputing* **2016**, *218*, 439–447. [[CrossRef](#)]
27. Xu, Y.; Luo, D.; You, Y.; Duan, H. Affine Transformation Based Formation Maneuvering for Discrete-Time Directed Networked Systems. *Sci. China Technol. Sci.* **2020**, *63*, 73–85. [[CrossRef](#)]
28. Zhao, S. Affine Formation Maneuver Control of Multiagent Systems. *IEEE Trans. Autom. Control* **2018**, *63*, 4140–4155. [[CrossRef](#)]
29. Zhang, Y.; Chen, M.; Chen, J.; Chen, C.; Yu, H.; Zhang, Y.; Deng, X. Time-Varying Topology Formation Reconfiguration Control of the Multi-Agent System Based on the Improved Hungarian Algorithm. *Appl. Sci.* **2023**, *13*, 11581. [[CrossRef](#)]
30. Tan, W.; Huang, N.; Huang, C.; Yu, C.; Zhong, C. Fixed-Time Rigidity-Based 3-D Formation Maneuvering Control with Distributed Finite-Time Velocity Estimators. In Proceedings of the 2019 Chinese Control Conference (CCC), Guangzhou, China, 27–30 July 2019; IEEE: Piscataway, NJ, USA, 2019; pp. 3237–3242.
31. Yang, Q.; Sun, Z.; Cao, M.; Fang, H.; Chen, J. Construction of Universally Rigid Tensegrity Frameworks and Their Applications in Formation Scaling Control. In Proceedings of the 2017 36th Chinese Control Conference (CCC), Dalian, China, 26–28 July 2017; IEEE: Piscataway, NJ, USA, 2017; pp. 8177–8182.
32. Gortler, S.J.; Thurston, D.P. Characterizing the Universal Rigidity of Generic Frameworks. *Discret. Comput. Geom.* **2014**, *51*, 1017–1036. [[CrossRef](#)]
33. Wu, G.; Hammers, J. Leader-Following Consensus of Nonlinear Discrete-Time Multi-Agent Systems with Limited Bandwidth and Switching Topologies. *Am. J. Clin. Pathol.* **2019**, *152*, S76. [[CrossRef](#)]
34. Yang, Q.; Cao, M.; Fang, H.; Chen, J. Constructing Universally Rigid Tensegrity Frameworks with Application in Multiagent Formation Control. *IEEE Trans. Autom. Control* **2019**, *64*, 381–388. [[CrossRef](#)]
35. Zhang, Y.; Chen, M.; Chen, J.; Chen, C.; Yu, H. Time-Varying Target Formation Control for Multi-agent Systems Based on Stress-Matrix. In *Advances in Mechanism, Machine Science and Engineering in China*; Lecture Notes in Mechanical Engineering; Liu, X., Ed.; Springer: Singapore, 2023.
36. Lyu, H.; Yin, Y. COLREGS-Constrained Real-Time Path Planning for Autonomous Ships Using Modified Artificial Potential Fields. *J. Navig.* **2019**, *72*, 588–608. [[CrossRef](#)]
37. Xiong, J.Q. Research on Consensus of Multi-UAV Route Planning Based on Artificial Potential Field. Ph.D. Thesis, Nanchang Hangkong University, Nanchang, China, 2017.
38. Zhao, H.B. Research on Key Problems of Multi-Agent Motion Formation Control. Master's Thesis, Inner Mongolia University of Science and Technology, Mongolia, China, 2019.
39. Jia, T.X. Research on Agent Path Planning and Formation Control. Master's Thesis, Yanshan University, Qinhuangdao, China, 2021.
40. Zhang, L.T. On Cooperative Control Algorithm of Heterogeneous Multi-Vehicle System. Master's Thesis, University of Electronic Science and Technology of China, Chengdu, China, 2022.
41. Sun, Y.; Zhou, J.; Wei, Y.; Fan, Z. Dynamic Flight Trajectory Planning of Distribution UAV Cluster Based on Artificial Potential Field. *J. Mil. Transp. Univ.* **2022**, *6*, 80–85.
42. Zhang, Y.C.; Jiang, Y.; Dai, J.Y. Dynamic Obstacle Avoidance Control of Three-order Multi-robot Cooperative Formation. *J. Syst. Simul.* **2022**, *34*, 1762–1774.
43. Yamakou, M.E. Chaotic Synchronization of Memristive Neurons: Lyapunov Function Versus Hamilton Function. *Nonlinear Dyn.* **2020**, *101*, 487–500. [[CrossRef](#)]
44. Han, Z.; Wang, L.; Lin, Z.; Zheng, R. Formation Control with Size Scaling Via a Complex Laplacian-Based Approach. *IEEE Trans. Cybern.* **2016**, *46*, 2348–2359. [[CrossRef](#)] [[PubMed](#)]
45. Zhao, P. Design of UAV Formation and Obstacle Avoidance Control System Based on Virtual Leader. Master's Thesis, University of Electronic Science and Technology of China, Chengdu, China, 2021.

**Disclaimer/Publisher's Note:** The statements, opinions and data contained in all publications are solely those of the individual author(s) and contributor(s) and not of MDPI and/or the editor(s). MDPI and/or the editor(s) disclaim responsibility for any injury to people or property resulting from any ideas, methods, instructions or products referred to in the content.